Polyhedron 44 (2012) 1–10

Contents lists available at SciVerse ScienceDirect

Polyhedron

journal homepage: www.elsevier.com/locate/poly

Synthesis and characterization of novel square planar copper(II)–dipeptide–1,10-phenanthroline complexes: Investigation of their DNA binding and cleavage properties

Pulimamidi Rabindra Reddy *, Nomula Raju

Department of Chemistry, Osmania University, Hyderabad 500 007, India

ARTICLE INFO

Article history:
Received 16 March 2012
Accepted 22 May 2012
Available online 28 June 2012

Keywords:
Bioinorganic chemistry
Cu(II) complexes
DNA binding
Hydrolytic cleavage
Oxidative cleavage

ABSTRACT

In view of the importance of aromatic moieties in DNA binding and cleavage, two new Cu(II)–dipeptide–phen (phen = 1,10-phenanthroline) complexes, viz. [Cu(II)(boc(tos)-his-trp-ome)(phen)]$(ClO_4)_2$ (**1**) and [Cu(II)(boc(tos)-his-tyr-ome)(phen)]$(ClO_4)_2$ (**2**) were synthesized, comprehensively characterized and their structures reported. The physico-chemical data and molecular modeling approaches support that the complexes are arranged in a distorted square planar geometry. To provide an insight on the mode and affinity of the interaction of these complexes with calf thymus (CT) DNA the following experiments were carried out: thermal denaturation (T_m), UV–Vis absorption, competitive binding, viscosity and fluorescence spectroscopy studies. These experimental results indicate that the complexes interact through stacking between the base pairs of double helix DNA. The overall binding constants (K_b) were determined as 3.33×10^4 and 2.82×10^4 M^{-1} for **1** and **2** respectively. The complexes converted supercoiled plasmid pUC19 DNA (SC DNA) into its nicked (NC) form both in the absence (hydrolytic cleavage) and presence (oxidative cleavage) of H_2O_2. The control experiments demonstrate that no diffusible radical species were involved in the hydrolytic cleavage, but in the presence of H_2O_2, hydroxyl radical ($OH^{\cdot}$) species were generated and initiated the cleavage reaction by an oxidative pathway. The rate constants for the hydrolysis of the phosphodiester bond were determined as 1.70 h^{-1} and 1.82 h^{-1} for **1** and **2** respectively. This amounts to a $(4.7–5.0) \times 10^7$-fold rate enhancement compared to non-catalyzed DNA cleavage, which is significant. These complexes exhibit better DNA binding and cleavage abilities compared to similar reported complexes.

1. Introduction

The design of artificial nucleases represents an area of substantial interest since nucleases have wider applications in molecular biology in probing the structures and functions of nucleic acids [1–4]. In contrast to natural DNA-binding enzymes, low molecular artificial nucleases exhibit higher stability and less reactive condition dependence when they are used as an accelerator in DNA cleavage [5,6].

Many studies suggest that DNA is an important primary cellular receptor. Many chemicals exert their antitumor effects by binding to DNA, thereby cleaving the DNA and inhibiting the growth of tumor cells, which is the basis for designing new and more efficient antitumor drugs, and their effectiveness depends on the mode and affinity of the binding [7–9]. Transition metal complexes that are capable of cleaving DNA under physiological conditions are of interest in the development of metal-based anticancer agents [10–12]. The clinical success of cisplatin and related platinum-based drugs, as anticancer agents that bind covalently to DNA, is severely affected by the serious side effects, general toxicity, and acquired drug resistance [13]. This is impetus to chemists to develop innovative strategies for the preparation of more effective, less toxic, target specific and preferably non-covalently bound anticancer drugs. In this regard, Cu(II) complexes are proving to be the most promising alternatives to cisplatin as anticancer drugs.

Planar heterocyclic base complexes have been at the forefront of these investigations because of their unusual electronic properties, diverse chemical reactivity, and peculiar structure, which results in non-covalent interactions with DNA. Copper, being a bio-essential transition metal ion, and its complexes, with tunable coordination geometries in a redox active environment, could find

Abbreviations: EDCI, 1-ethyl-3-(3-dimethylaminopropyl)carbodiimide); HOBt, hydroxybenzotriazole; TFA, trifluoroacetic acid; His-trp, histidyl-tryptophan; His-tyr, histidyl-tyrosine; phen, 1,10-phenathroline; CT-DNA, calf-thymus DNA; Tris, Tris(hydroxymethyl)aminomethane; EB, ethidium bromide; UV–Vis, ultraviolet–visible; DMSO, dimethyl sulfoxide; **1**, [Cu(II)(boc(tos)-his-trp-ome)(phen)]$(ClO_4)_2$; **2**, [Cu(II)(boc(tos)-his-tyr-ome)(phen)]$(ClO_4)_2$.

* Corresponding author. Tel.: +91 40 27171664; fax: +91 40 27090020, 27097099.

E-mail address: profprreddy@gmail.com (P.R. Reddy).

0277-5387/$ - see front matter © 2012 Elsevier Ltd. All rights reserved.
http://dx.doi.org/10.1016/j.poly.2012.05.046

better applications at the cellular level. Amino acids/peptides are the basic structural units of proteins that recognize a specific base sequence of DNA. An amino acid with a side chain aromatic ring, e.g. phenylalanine, tryptophan, tyrosine, etc., contributes mainly to the stabilization of proteins through hydrophobic interactions and the formation of hydrophilic environments [14,15].

In earlier publication [16], we isolated copper complexes of histidine containing dipeptides with aliphatic side chains, i.e. $[Cu^{II}(HisLeu)(phen)]^+$ and $[Cu^{II}(HisSer)(phen)]^+$, and studied their DNA binding and cleavage properties. Since aromatic moieties are known to play an important role in enhancing DNA binding and cleavage activity, we extended our study to dipeptides with aromatic side chains. Here we report the synthesis, characterization, DNA binding, hydrolytic and oxidative DNA cleavage activity of two new complexes, [Cu(II)(boc(tos)-his-trp-ome)(phen)]$(ClO_4)_2$ (**1**) and [Cu(II)(boc(tos)-his-tyr-ome)(phen)]$(ClO_4)_2$ (**2**). Compared to aliphatic dipeptide complexes, the aromatic dipeptide complexes show better DNA binding and cleavage activity. This reveals the importance of aromatic moieties in DNA binding and cleavage.

2. Experimental

2.1. Materials and instruments

EDCI, HOBt, DIPEA, TFA, $LiOH{\cdot}H_2O$, boc(tos)-histidine, tryptophan methyl ester, tyrosine methyl ester, $Cu(OAc)_2{\cdot}H_2O$, acetic acid, EDTA, phen and ethidium bromide (EB) were obtained from Sigma (99.99% purity) USA and were of analar grade. The peptides (boc(tos)-his-trp-ome and boc(tos)-his-tyr-ome) were synthesized by the conventional solution phase method [17]. CT-DNA was obtained from Fluka (Switzerland). Supercoiled plasmid pUC19 DNA, agarose, Tris–HCl and Tris base were obtained from Bangalore Genei (India). Solvents (MeOH, CH_2Cl_2 and THF) were purchased from Merck, India and all the chemicals were used as supplied. The spectroscopic titrations were carried out in aerated buffer (5 mM Tris–HCl/50 mM NaCl, pH 7.5) at room temperature (r.t.).

Elemental analyses data were obtained from the microanalytical Heraeus Carlo Erba 1108 elemental analyzer. The copper content was determined on a Shimadzu AA-6300 atomic absorption spectrophotometer. The molar conductivity was measured on a Digisun digital conductivity bridge (model: DI-909) with a dip type cell. Infrared spectra were recorded on a Perkin Elmer FT-IR spectrometer, in KBr pellets in the 4000–400 cm^{-1} range. Magnetic moments of the complexes were recorded at room temperature on a Faraday balance (CAHN-7600) using $Hg[Co(NCS)_4]$ as the standard. Diamagnetic corrections were made using Pascal's constants [18]. ESI mass spectra of the complexes were recorded using a Quattro Lc (Micro Mass, Manchester, UK) triple quadruple mass spectrometer with MassLynx software. UV–Vis spectra of the complexes were recorded on a Jasco V-530 UV–Vis spectrophotometer using 1 cm quartz micro-cuvettes. TGA analyses were obtained by a METLER TOLEDO (TGA/SDTA 851^e) thermo analyzer at 25–300 °C, with a heating rate of 5 °C/min. The molecular modeling calculations were carried out with a semi-empirical PM3 Hamiltonian as implemented in the hyperchem 6.0 software program package. The DNA cleavage experiments conducted using Genei (India) gel-electrophoresis equipment. The gel pattern of the electrophoresis was photographed by the Alpha-Innotec gel documentation system (USA).

2.2. Synthesis of the peptides and Cu(II) complexes

2.2.1. boc(tos)his-trp-ome and boc(tos)his-tyr-ome

The dipeptides (boc(tos)-his-trp-ome and boc(tos)-his-tyr-ome) were synthesized by adopting EDCI and HOBt as coupling agents in the presence of DIPEA and with dry CH_2Cl_2 as the solvent.

[boc(tos)-his-trp-ome]: ^{1}H NMR (400 MHz, $CDCl_3$), δ: 1.40 (s, 9H), 2.34 (m, 3H), 2.93–3.90 (s, 7H), 4.40–4.95 (m, 2H), 7.10–7.85 (m, 10H), 8.03 (m, 2H), 8.05 (m, 1H), 10.10 (m, 1H); ESI-MS, *m*/*z*: 609.

[boc(tos)-his-tyr-ome]: ^{1}H NMR (400 MHz, $CDCl_3$), δ: 1.40 (s, 9H), 2.34 (m, 3H), 2.80–3.90 (s, 7H), 5.30 (m, 1H), 4.40–4.95 (m, 2H), 6.65–7.85 (m, 9H), 8.03 (m, 2H), 8.05 (m, 1H); ESI-MS, *m*/*z*: 586.

2.2.2. [Cu(II)(boc(tos)-his-trp-ome)(phen)]$(ClO_4)_2$ (**1**) and [Cu(II)(boc(tos)-his-tyr-ome)(phen)] $(ClO_4)_2$ (**2**)

To a methanolic solution of boc-(tos)his-trp-ome (0. 609 g, 1.0 mM) for **1** or boc-(tos)his-tyr-ome (0.586 g, 1.0 mM) for **2**, a methanolic solution of $Cu(OAc)_2{\cdot}H_2O$ (0.198 g, 1.0 mM) was added under stirring, followed by the addition of phen (0.198 g, 1.0 mM) in MeOH (5 mL). The reaction was continued for ca. 6 h at room temperature and then an aq. solution of $NaClO_4{\cdot}H_2O$ (0.36 g, 2.0 mM) was added. A yellow precipitate was isolated and it was filtered and washed with ether, and then dried.

***[1]**: Anal.* Calc. for $C_{42}H_{43}Cl_2CuN_7O_{15}S$: C, 47.94; H, 4.12; N, 9.32; Cu, 6.04. Found: C, 47.89; H, 4.10; N, 9.28; Cu, 6.00%. IR (KBr, cm^{-1}): 3340br, 2926m, 1711m, 1665s, 1585s, 1518s, 1428s, 1366m, 1222m, 1166s, 1107m, 1034m, 1010s, 847s, 818m, 722s, 681m, 568m, 429s. UV–Vis [λ nm; MeOH:H_2O (1:10)]: 550, 395, 269, 212. ESI-MS *m*/*z*: 853 $[M+H]^+$. MP: 250 °C. μ_{eff} = 1.78 BM. Λ_M [Ω^{-1} cm^2 M^{-1}, 10^{-3} M in MeOH:H_2O (1:10), 25 °C]: 120. Yield: ~85%.

***[2]**: Anal.* Calc. for $C_{40}H_{42}Cl_2CuN_6O_{16}S$: C, 46.67; H, 4.11; N, 8.16; Cu, 6.17. Found: C, 46.63; H, 4.08; N, 8.12; Cu, 6.10%. IR (KBr, cm^{-1}): 3349br, 2926s, 1665s, 1597m, 1502m, 1426s, 1365m, 1244m, 1176m, 1092m, 955m, 867s, 745s, 723m, 553m, 429s. UV–Vis [λ nm; MeOH:H_2O (1:10)]: 540, 394, 268, 204. ESI-MS *m*/*z*: 830 $[M+H]^+$. MP: 265 °C; μ_{eff} = 1.76 BM. Λ_M [Ω^{-1} cm^2 M^{-1}, 10^{-3} M in MeOH:H_2O (1:10), 25 °C]: 150. Yield: ~85%.

2.3. DNA binding

2.3.1. Preparation of stock solution

Concentrated CT-DNA stock solution was prepared in 5 mM Tris–HCl/50 mM NaCl in double distilled water at pH 7.5 and the concentration of the DNA solution was determined by UV absorbance at 260 nm (ε = 6600 M^{-1} cm^{-1}) [19]. A solution of CT-DNA in 5 mM Tris–HCl/50 mM NaCl (pH 7.5) gave a ratio of UV absorptions at 260 and 280 nm A_{260}/A_{280} of ca. 1.8–1.9, indicating that the DNA was sufficiently free of protein [20]. All stock solutions were stored at 4 °C and were used within 4 days. The concentration of EB was determined spectrophotometrically at 480 nm (ε = 5680 M^{-1} cm^{-1}) [21].

2.3.2. Thermal denaturation (T_m) studies

Thermal denaturation studies were performed on a Shimadzu 160A spectrophotometer equipped with a thermostatic cell holder. The T_m value of CT-DNA was determined in the absence and presence of Cu(II) complexes by keeping the concentration of DNA and complexes **1** and **2** (30 μM) in a 1:1 ratio. The DNA samples were continuously heated at the rate of 1 °C/min temperature increase, while the absorption changes at 260 nm were monitored. The melting temperature (T_m), which is defined as the temperature where half of the total base pairs are unbound, was determined from the midpoint of the melting curves. ΔT_m values were calculated by subtracting T_m of free DNA from T_m of DNA interacting with the complex [22].

2.3.3. UV–Vis absorption spectroscopy

Absorption spectra were recorded on Jasco V-530 UV–Vis spectrophotometer using 1 cm quartz micro-cuvettes. Absorption titrations were performed by keeping the concentration of the

complexes constant (10 μM), and by varying the concentration of CT-DNA from 0 to 10 μM. In the reference cell, a DNA blank was placed so as to cancel any absorbance due to DNA at the measured wavelength. For complexes **1** and **2**, the binding constants (K_b) were determined from the spectroscopic titration data using the following equation [23,24]:

$$[DNA]/(\varepsilon_a - \varepsilon_f) = [DNA]/(\varepsilon_b - \varepsilon_f) + 1/K_b(\varepsilon_b - \varepsilon_f) \quad (1)$$

The 'apparent' extinction coefficient (ε_a) was obtained by calculating A_{obsd}/[Cu]. The terms ε_f and ε_b correspond to the extinction coefficients of free (unbound) and the fully bound complexes, respectively. A plot of [DNA]/($\varepsilon_a - \varepsilon_f$) versus [DNA] will give a slope of 1/($\varepsilon_b - \varepsilon_f$) and an intercept of 1/$K_b$($\varepsilon_b - \varepsilon_f$). K_b is the ratio of the slope to the intercept.

2.3.4. Competitive binding

The competitive binding experiments were performed on a Jasco V-530 UV–Vis spectrophotometer using 1 cm quartz microcuvettes. Absorption titrations were performed for complexes **1** and **2** by keeping the concentration of EB (40 μM) and DNA (40 μM) constant, and by varying the complex concentration from 0 to 40 μM.

2.3.5. Viscosity

Viscometric titrations were performed with an Ostwald Viscometer at room temperature for EB (standard), **1** and **2**. The concentration of DNA was 200 μM, the EB and complex concentrations were varied from 0 to 200 μM and the flow times were measured with a digital timer. Each sample was measured three times for accuracy, and an average flow time was determined. Data is presented as $(\eta/\eta_o)^{1/3}$ versus [complex]/[DNA], where η is the viscosity of DNA in the presence of complex and η_o that of DNA alone. Viscosity values were calculated from the observed flow time of DNA containing solutions (t) corrected for that buffer alone (t_o), $\eta = (t - t_o)$.

2.3.6. Fluorescence spectroscopy

Fluorescence spectra were recorded with a SPEX-Fluorolog 0.22 m fluorimeter equipped with a 450 W Xenon lamp. The slit widths were 2 × 2 × 2 × 2 and the emission spectral range was 550–650 nm. A solution containing DNA and EB was titrated with varying concentrations of **1** and **2**. The concentration of DNA and EB was maintained at 41 μM and the concentration of complexes was in the range 0–196 μM. The solutions containing DNA and EB were mixed (equimolar ratio) and the complexes **1** and **2** were added and allowed to equilibrate. They were excited at 540 nm (λ_{max} for EB) and the fluorescence emission at 598 nm (λ_{max}) was recorded.

Fluorescence spectra were also utilized to obtain *Scatchard* plots. For this, titrations of DNA against EB in the absence and presence of the complexes were performed. The initial concentration of DNA was 20 μM and the concentrations of **1** and **2** were kept at 50 μM. After each addition of EB to the solutions containing DNA and the complexes, the emission spectra were recorded in the range 550–650 nm with excitation at 540 nm at 25 °C. Corrections were made to the data for the volume changes during the course of the titrations. The data were analyzed by the method of Lepecq and Paoletti [25] to obtain the bound (c_b) and free (c_f) concentration of EB, and *Scatchard* plots were obtained by plotting r_{EB}/c_f versus r_{EB} (where $r = c_b/[DNA]$).

2.4. DNA cleavage

Electrophoresis experiments were performed using supercoiled pUC19 plasmid DNA according to the established procedures. The cleavage of supercoiled (SC) DNA (38 μM base pair concentration) was accomplished by the addition of Cu(II) complexes **1** and **2** in the absence ([**1** and **2**] = 50, 100 and 150 μM) and presence ([**1** and **2**] = 5 and 10 μM) of 1 mM H_2O_2, dissolved in 5 mM Tris buffer at pH 7.2. The mixtures were incubated at 37 °C for a period of 3 h. The reactions were quenched and the resulting solutions were subjected to electrophoresis. The analysis involved loading of the solutions onto 1% agarose gels containing 2.5 μM EB (2 μL), and the DNA fragments separated by gel electrophoresis (60 V for 2 h in standard Tris–acetate–EDTA (TAE) buffer, pH 8). EB-stained agarose gels were imaged, and densitometric analysis of the visualized bands was used to determine the extent of supercoiled DNA cleavage.

Control experiments were carried out using $Cu(OAc)_2{\cdot}H_2O$ and the free ligands at a concentration of 1 mM. For investigation of the mechanistic aspects, the cleavage of SC DNA was also carried out in the presence of 1 mM DMSO, a standard hydroxyl radical scavenger. The reaction conditions used were Cu(II) complex [150 μM for hydrolytic and 10 μM + 1 mM H_2O_2 for oxidative cleavage] and 38 μM base-pair concentration of supercoiled plasmid DNA. Each solution was incubated at 37 °C for 3 h and analyzed according to the procedure described above. For evaluating kinetic aspects, the complex concentration was fixed at 300 μM with different incubation times (0–120 min) under identical experimental conditions.

3. Results and discussion

3.1. Synthesis and solubility

The primary dipeptide ligands were synthesized by a conventional solution phase method [17] in DCM in the presence of EDCI and HOBt as coupling agents, and their ternary Cu(II) complexes (**1** and **2**) were isolated on reaction with Cu(II) acetate monohydrate in methanol, with phen as a secondary ligand (Scheme 1). The complexes show good solubility in MeOH/EtOH:H_2O (1:10) mixture. They are non-hygroscopic and are stable in both solid and solution phases. The analytical data for the Cu(II) complexes were in good agreement with the molecular formula of the complexes. The molar conductance values (Table 1) are in the range for 1:2 electrolytes, no further dissociation of the complex species ($[Cu(II)(boc(tos)\text{-}his\text{-}trp\text{-}ome)(phen)]^{2+}$ and $[Cu(II)(boc(tos)\text{-}his\text{-}tyr\text{-}ome)(phen)]^{2+}$ was observed. The observed magnetic moment values (μ_{eff} = 1.74 and 1.70 BM for **1** and **2** respectively) are in the range for a one unpaired electron system with spin (1/2), which represents the paramagnetic nature of the Cu(II) complexes [26].

3.2. Characterization of the complexes

3.2.1. IR spectra

The assignments of the infrared spectra were made on the basis of literature and Nakamoto [27]. The IR spectra of **1** and **2** were analyzed in comparison with their free ligand spectra. The ν(N–H) vibration of the free peptides, observed at 3301 cm^{-1} for his-trp and 3390 cm^{-1} for his-tyr (Fig. S1), were shifted to 3340 cm^{-1} for **1** and 3381 cm^{-1} for **2** upon complexation with copper (Fig. S2). Similarly the imidazole ν(C=N) peak at 1674 cm^{-1} was shifted to 1665 cm^{-1} on interaction with Cu(II) in both complexes, which can be attributed to the coordination of nitrogen atoms of the amine and imino groups to copper. The peaks corresponding to the free phen ring stretching frequencies ν(C=C) and ν(C=N), observed at 1502 and 1421 cm^{-1}, were shifted to 1518 and 1428 cm^{-1} respectively, and the low energy pyridine ring characteristic in plane and out-of-plane hydrogen bending modes of free phen, observed at 853 and 738 cm^{-1}, were shifted to 848 and 722 cm^{-1} respectively for **1** and **2**, which is a good indication of the coordination of the heterocyclic nitrogen to copper [27].

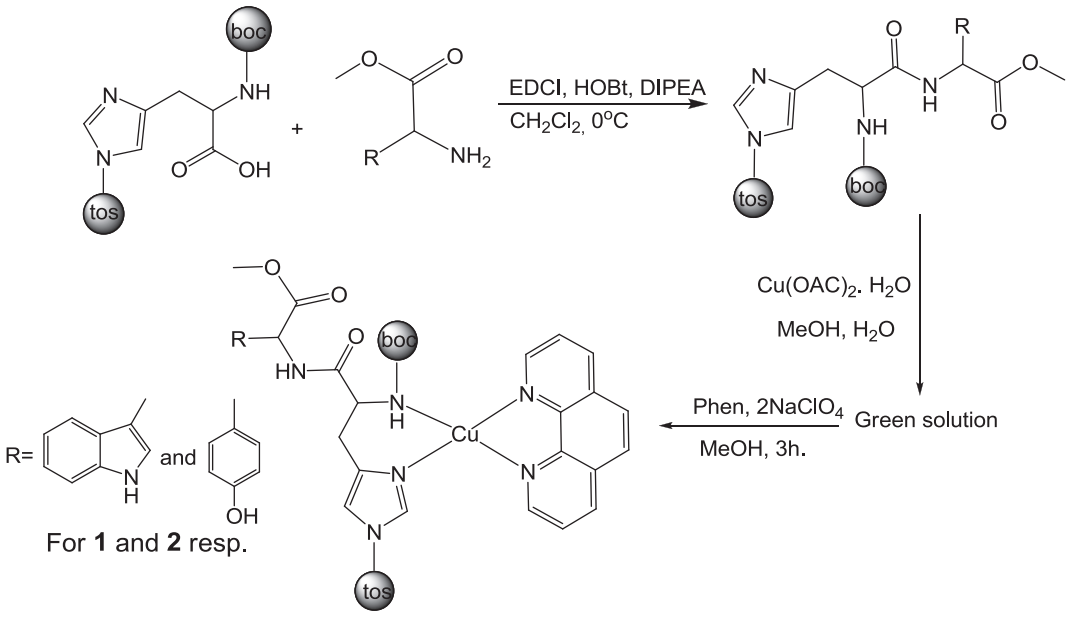

Scheme 1. General approach for the synthesis of peptides and the Cu(II) complexes **1** and **2**.

Table 1
Physico-chemical data for complexes **1** and **2**.

Complex	IR (cm^{-1})			μ_{eff} (BM)	ESI-MS	UV–Vis (nm)	Λ_M (Ω^{-1} cm^2 M^{-1})	MP (°C)
	ν(N–H)	ν(C=N)	ν(M–N)					
1	3340	1674	568	1.78	853	550, 395, 269, 212	120	250
2	3381	1674	553	1.76	830	540, 394, 268, 204	150	265

The very strong single band at 1086 cm^{-1} for **1** and 1094 cm^{-1} for **2** were assigned to ν(Cl–O) of perchlorate anions, satisfying the Werner's primary valence of the complexes [28]. The new non-ligand peaks at 568 cm^{-1} for **1** and 553 cm^{-1} for **2** were assigned to ν(Cu–N) vibrations [29], which also indicates that the ligands are coordinated to copper through nitrogen atoms.

3.2.2. Electronic spectra

In the electronic spectra of the Cu(II) complexes, four absorption bands with varied intensities were observed for **1** (Fig. 1) and **2** (Fig. S3) in MeOH:H_2O solution. The intense bands at 212 and 269 nm for **1** and 206 and 268 nm for **2** were assigned to intra-ligand (π–π^*) transitions of the phen ligand, while the less intense band at 395 nm for **1** and **2** was assigned to LMCT transitions. Additionally, much weaker, less well defined broad bands observed in the lower energy regions at 550 and 540 nm for **1** and **2** respectively were assigned to d–d [$^2B1g \rightarrow {}^2Eg - (\nu_1)(d_{x^2-y^2} \rightarrow d_{yz})$] transitions. These transitions represent a distorted square-planar geometry. This agrees well with the reported square-planar Cu(II) complexes [30].

3.2.3. Mass spectra

The active chemical species of the complexes were identified by means of electrospray ionization mass spectrometry (ESI-MS). The mass to charge ratio peaks observed at m/z 853 and 830 were due to the formation of the species [Cu(II)(boc(tos)-his-trp-ome)(phen)]$^{2+}$ for **1** (Fig. S4) and [Cu(II)(boc(tos)-his-tyr-ome)(phen)]$^{2+}$ for **2** respectively (Fig. S5). These molecular ion species are responsible for all the properties shown by the complexes.

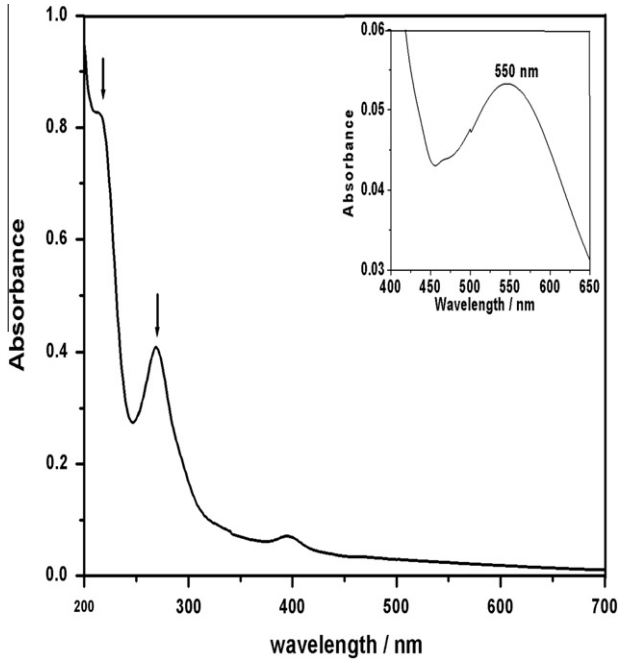

Fig. 1. Electronic absorption spectrum of **1**. Insets: d–d transition.

3.2.4. Thermo gravimetric analysis (TGA)

Normally, the amide group of histidine containing dipeptide ligands is not involved in metal coordination, especially at physiological pH. However, it is possible to have a five coordination geometry around copper with one water (H_2O) molecule in the coordination sphere. To examine the presence of water molecules in the present complexes, they were subjected to thermo gravimetric analysis (TGA).

Water molecules present in the crystal lattices of complexes are generally of two types – lattice water (non-coordinated to the

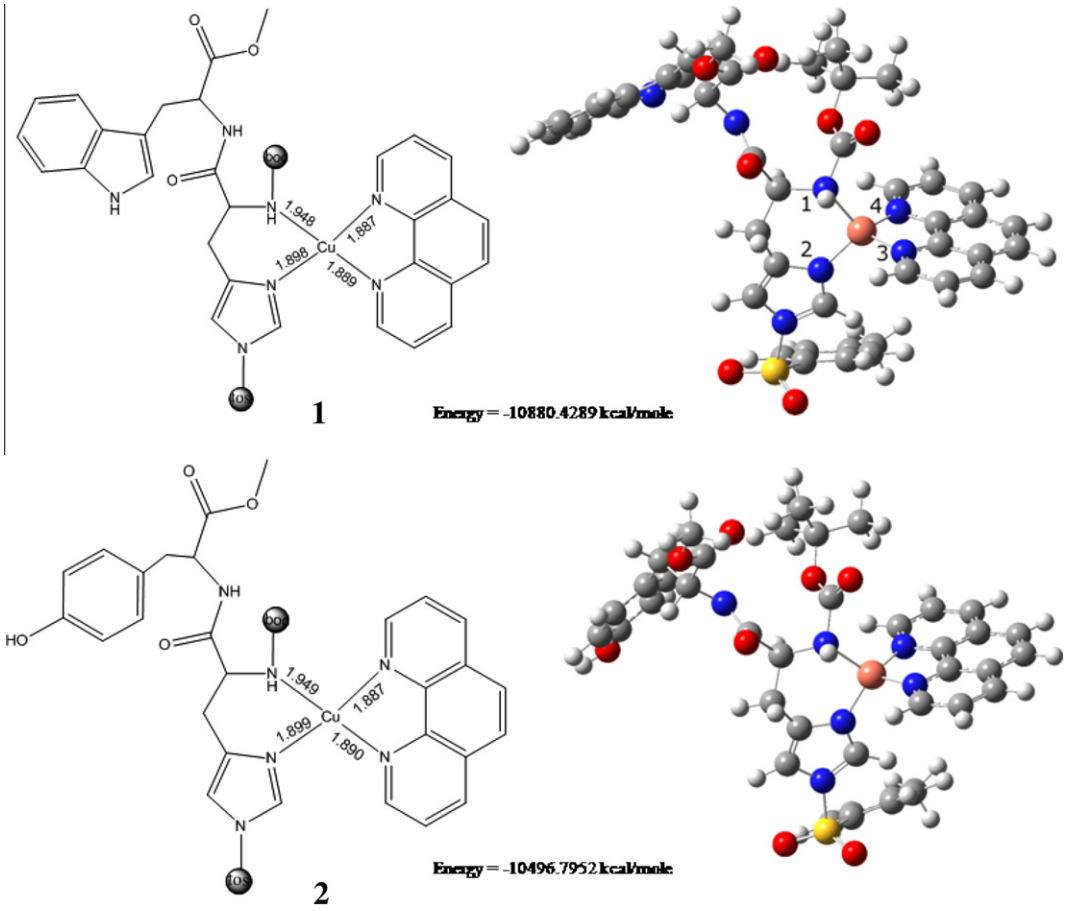

Fig. 2. Proposed geometry and energy-minimized molecular structures, relative energies and bond lengths of **1** and **2**.

metal ion) and coordinated water. The lattice water will be lost at low temperatures (90–150 °C), whereas the loss of coordinated water molecule is observed at high temperatures (150–250 °C). The thermal decomposition stoichiometry of the analytically characterized complexes was determined by thermo gravimetric analysis (TGA). The thermal behavior of the complexes was monitored up to 500 °C in a nitrogen atmosphere. In the case of complexes **1** (Fig. S6) and **2** (Fig. S7), no weight loss was observed in the above mentioned temperature ranges. This suggests that there is no evidence for the presence of water molecules in the complexes. Based on the literature, electronic spectra and TGA data, a distorted square-planar geometry was confirmed for the complexes. The complexes decomposed above 350 °C.

3.2.5. Molecular modeling studies

In the absence of crystal data, it was thought worthwhile to obtain structural information through molecular modeling. Molecular mechanics, which provides the energy minimized conformation, is a tool of increasing importance for the structural investigation of coordination and organometallic compounds. These were carried out with the semi-empirical PM3 Hamiltonian as implemented in the hyperchem 6.0 software program package. The ball and stick representations of complexes **1** and **2** are shown in Fig. 2. As can be seen from the figure, the complexes are arranged in a distorted square-planar geometry at their minimum energy state. These results also support distorted square-planar geometries for the present complexes. The relative minimum energies and relevant bond lengths for the complexes are also provided.

3.3. DNA binding

The Cu(II) complexes can bind to the double stranded (ds) DNA in different modes on the basis of their structure, charge and type of ligands. To identify the mode of binding involved between the complexes and ds-DNA, the biophysical methods of thermal denaturation, UV–Vis absorption spectra, competitive binding study, viscosity, fluorescence spectroscopy and gel-electrophoresis were adopted.

3.3.1. Thermal denaturation studies

DNA melting studies were used in predicting the nature of binding and relative binding strength of metal complexes to the DNA [31]. The denaturation temperatures of free and copper complex-bound CT-DNA were examined. The melting of the helix can lead to an increase in the absorption at 260 nm, because the extinction coefficient of DNA bases at 260 nm in the double helical form is much less than in the single strand form [32–37]. Thus, the helix to coil transition temperature T_m, can be determined by monitoring the absorbance of the DNA bases at 260 nm as a function of temperature. The interaction of small molecules with double-helical DNA may increase or decrease T_m, the temperature at which the double helix is broken up into a single-stranded DNA. While an increase in T_m values suggests intercalative or phosphate binding, a decrease is typical for base binding. The thermal denaturation profile of DNA in the absence and presence of the complexes is provided in Fig. 3. As can be seen, an increase of ~6 °C for **1** and **2** was observed in the T_m profile of the complexes as compared to free DNA. This increase in the helix melting temperature indicates the

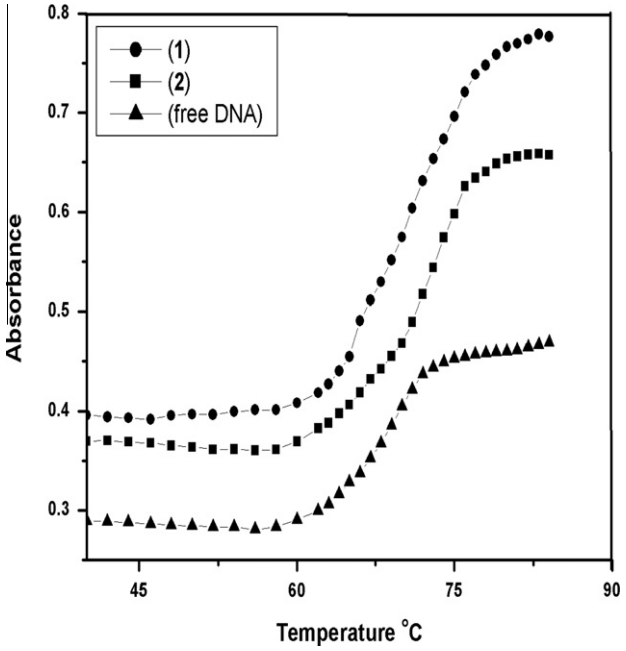

Fig. 3. Thermal denaturation profiles of free CT-DNA (▲) and in the presence of **1** (●) and **2** (■). [The concentrations of **1** or **2** and DNA were 30 μM.]

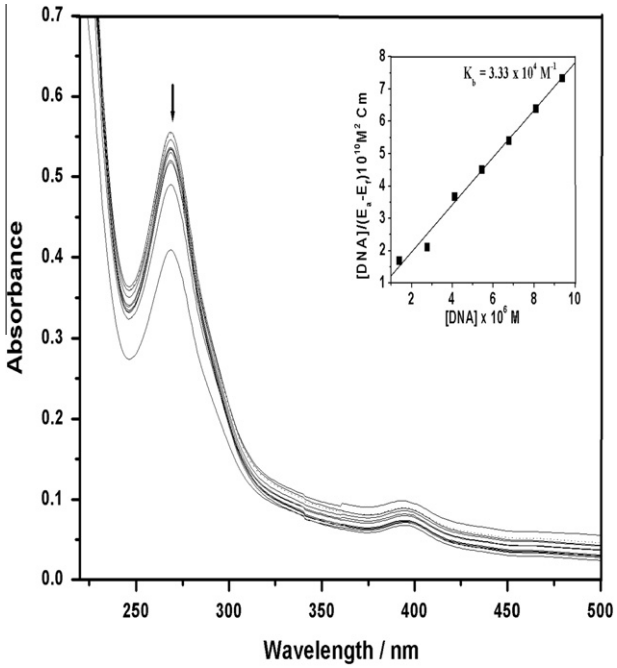

Fig. 4. Absorption spectra of **1** in the absence (···) and presence (—) of increasing amounts of CT-DNA. Conditions: [complex] = 10 μM. The arrow (↓) shows the absorbance changes upon increasing the DNA concentration. Inset: linear plot for the calculation of the intrinsic DNA binding constant (K_b).

increased stability of the double helix when these complexes bind to DNA. This provides a clear evidence for intercalative or phosphate binding of the copper complexes with DNA.

3.3.2. UV–Vis absorption spectroscopy

To further investigate the mode of binding between the complexes and the DNA double helix, UV-absorption studies were carried out. Monitoring the changes in the absorption spectra of the metal complexes upon addition of increasing amounts of DNA is one of the most widely used methods for determining the overall binding constants. Any interaction between the complex and DNA is expected to perturb the ligand centered spectral transitions of the complex. The absorption intensity of the complexes may decrease (hypochromism) or increase (hyperchromism) with a slight increase in absorption wavelength (bathochromism) in the presence of DNA. In general, it is assumed that hypochromism and bathochromism are related to association (intercalation) of the complex species with DNA [38,39]. The absorption spectra of **1** in the absence and presence of CT-DNA are illustrated in Fig. 4. On addition of increasing amounts of DNA to the complexes, the hypochromic (23%) (19% for **2**, Fig. S8) along with minor bathochromic shifts from 269–274 nm (268–272 nm for **2**) were observed. The hypochromism and bathochromism were suggested to arise due to the interaction between the electronic state of an intercalating chromophore (complex) and those of the DNA bases [40,41], i.e. the π^* orbital of the intercalated ligand can couple with the π orbital of the base pairs, thus decreasing the π–π^* transition energy and the resulting bathochromism. Moreover the coupling π orbital is partially filled by electrons, thus decreasing the transition probabilities and concomitantly resulting in hypochromism. The extent of the hypochromism is commonly consistent with the strength of the intercalative binding. The observed spectroscopic changes are thus consistent with intercalation of **1** and **2** into the DNA base stacks. In order to compare the binding strengths of the complexes, the intrinsic binding constant (K_b) for the association of the complexes with CT-DNA (insets of the respective figures) were determined using Eq. (1) (see Section 2) as $3.33 \times 10^4\ M^{-1}$ and $2.82 \times 10^4\ M^{-1}$ for **1** and **2** respectively. A slightly higher binding affinity of **1** than **2** for intercalative DNA binding is related to the presence of an extended aromatic indole ring of the coordinated his-trp, making the non-covalent interaction of the π system of the ligand with the DNA base pair more favorable and intimate than that of the phenyl ring of his-tyr in **2**. A larger aromatic moiety always facilitates potential intercalative DNA binding.

3.3.3. Competitive binding

Intercalative binding was also demonstrated through competitive binding experiments by UV–Vis spectroscopy using EB, a typical indicator of intercalation [42]. The study involves the addition of the complexes to DNA pre-treated with EB and subsequent measurement of the intensity of absorption. Free EB absorbs around 480 nm, but on interaction with DNA the absorption intensity decreases and the peak maximum shifts to a higher wavelength [43], which is characteristic of intercalation of EB into DNA base stacks. Fig. 5 shows that the maximal absorption of EB at 478 nm decreased and shifted to 481 nm in the presence of DNA, due to the intercalation of EB into the DNA base pairs. On addition of **1** in increasing amounts, a continuous increase in absorption was observed and the peak maximum was restored to its original position. This suggests that the complex displaces DNA-bound EB and occupies the intercalation sites on DNA, similar to that of EB. Similar trends were obtained for **2** (Fig. S9).

3.3.4. Viscosity

Optical or photo-physical properties are necessary but not sufficient to establish the mode of binding between the metal complexes and DNA. Hence viscosity measurements were carried out to further verify the mode of interaction of the metal complexes towards DNA. A hydrodynamic measurement, such as viscosity, is sensitive to length change and is regarded as the least ambiguous and the most critical test of a binding model in solution in the absence of crystallographic structural data [44,45]. A classical intercalation model demands that the DNA helix must lengthen as base pairs are separated to accommodate the binding ligand/

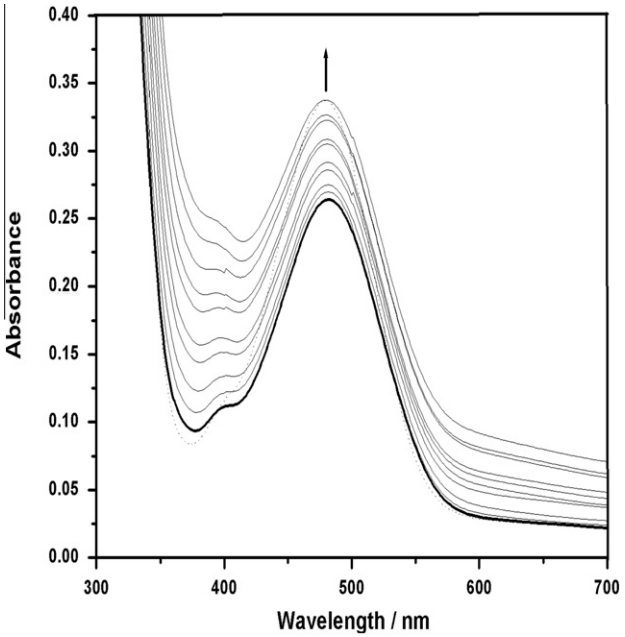

Fig. 5. Absorption spectra of free EB (···) and EB bound to CT-DNA in the absence (---) and presence (—) of increasing amount of **1**. Conditions: [EB] = 40 μM, [DNA] = 40 μM, [**1**] = (0–40 μM). The arrow (↑) shows the absorbance changes upon increasing the complex concentration.

complex, leading to an increase of DNA viscosity. In contrast, a partial intercalation of the ligand/complex could bend (or kink) the DNA helix, reduce its effective length and concomitantly its viscosity. The effect of EB, **1** and **2** on the viscosity of DNA at room temperature is shown in Fig. 6. The viscosity of the DNA increases steadily with increasing concentration of the complexes. This behavior is comparable with EB, which increases the relative specific viscosity by lengthening the DNA double helix as a result of intercalation. The results clearly emphasize that both the complexes intercalate between adjacent DNA base pairs, causing an extension in the helix and thereby increasing the viscosity of DNA [46].

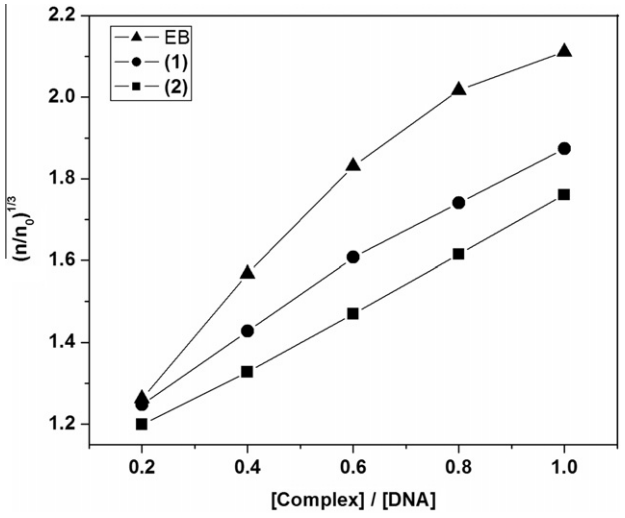

Fig. 6. Effect of increasing amounts of EB (▲), **1** (●) and **2** (■) on the relative viscosities of CT-DNA at room temperature in Tris–HCl buffer. Conditions: [DNA] = 200 μM, [EB, **1** and **2**] = 0–200 μM.

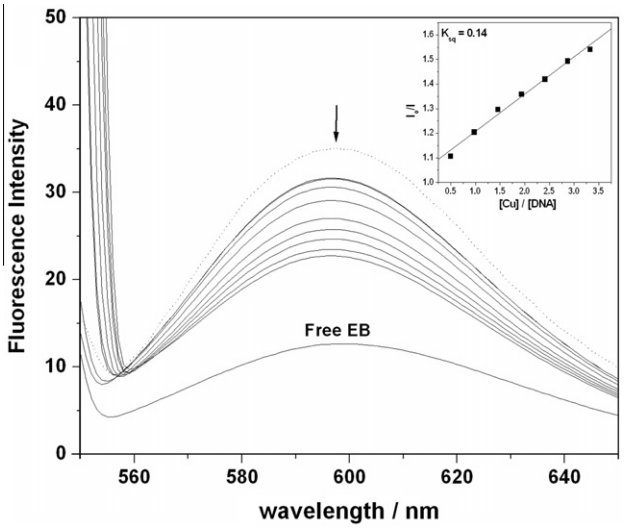

Fig. 7. Emission spectra of EB bound to CT-DNA in the absence (···) and presence (—) of complex **1**. [**1**/DNA = 0, 0.8, 1.60, 2.41, 3.19, 3.97, 4.78, λ_{ex} = 540 nm, Inset: Stern–Volmer quenching curve.]

3.3.5. Fluorescence spectroscopy

Competitive binding experiments with a well established fluorescence quenching experiment based on the displacement of the intercalating drug EB from CT-DNA may give further information about the relative binding affinity of the complexes to CT-DNA with respect to EB. EB is a classical intercalator that gives significant fluorescence emission intensity when it intercalates into the base pairs of DNA. When it is replaced or excluded from the internal hydrophobic circumstance of the DNA double helix by other small molecules, its fluorescence emission is effectively quenched by external polar solvent molecules such as H_2O [47]. The fluorescence quenching curves of EB bound to DNA in the absence and presence of **1** are given in Fig. 7.

As shown in Fig. 7, the EB–DNA system shows a characteristic strong emission at about 598 nm when excited at 540 nm, indicating that the intercalated EB molecules have been successfully protected by the neighboring DNA base pairs from being quenched by H_2O. A remarkable reduction in emission intensity was observed as **1** was added to the EB–DNA system, characteristic for the intercalative binding of **1** with DNA. Similar trends were observed for **2** (Fig. S10). The quenching efficiency for each complex was evaluated by the Stern–Volmer constant K_{sq}, which varies with the experimental conditions [48]:

$$I_o/I = 1 + K_{sq}.r$$

where I_o and I are the fluorescence intensities in the absence and presence of the complex, respectively, and r is the concentration ratio of the complex to DNA. K_{sq} is the linear Stern–Volmer quenching constant. The quenching plots illustrate that the quenching of emission of the EB–DNA system by the complexes is in good agreement with the linear Stern–Volmer equation, which also indicates that the complexes bind to DNA. The K_{sq} value is obtained as the ratio of the slope to intercept. The K_{sq} values for complexes **1** and **2** are 0.14 and 0.13 respectively (insets of the respective figures).

Fluorescence *Scatchard* plots for the binding of EB to CT-DNA in the presence of the complexes were obtained as described by Lepecq and Paoletti [25]. From the *Scatchard* plots, the complexes can be classified as exhibiting Type A or Type B behavior. Type A behavior produces a *Scatchard* plot in which the slope decreases in the presence of increasing amounts of metal complex, with no change in the intercept on the abscissa, indicating competitive inhibition of EB binding, viz. intercalation [49,50]. Type B behavior

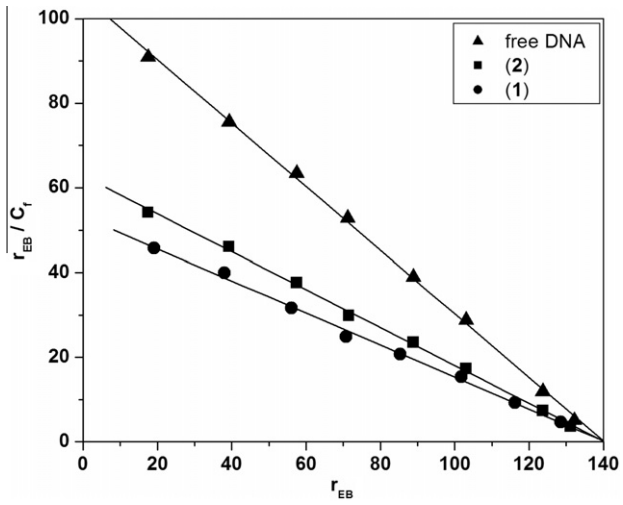

Fig. 8. Fluorescence *Scatchard* plots for EB bound to CT-DNA in the absence (▲) and presence of **1** (●) and **2** (■). The term r_{EB} is the concentration ratio of bound EB to total DNA and c_f is the concentration of free EB.

illustrates both the slope and intercept changing, with complexes exhibiting both intercalative and covalent interactions with DNA [51]. The binding isotherms of EB and DNA in the absence and presence of **1** and **2** were determined experimentally and are presented in Fig. 8. As can be seen from the plots, a decrease in slope with no change in the intercept resulted upon the addition of **1** and **2**, indicating an intercalative binding of the complexes with DNA. Thus the results obtained from the *Scatchard* plots validate those obtained from absorption, viscosity and emission spectral studies.

3.4. DNA cleavage studies

Agarose gel electrophoresis assay, a useful method to investigate various binding modes of small molecules to supercoiled DNA, also supports the above intercalative binding mode. Intercalation of small molecules to plasmid DNA can loosen or cleave the SC DNA form, which decreases its mobility rate and can be separately visualized by the agarose gel electrophoresis method, whereas a simple electrostatic interaction of small molecules to DNA does not significantly influence the SC form of DNA, thus the mobility of the SC form of DNA does not change. These results also confirm that the complexes bind to DNA.

The cleavage of supercoiled plasmid pUC19 DNA (2 μL) by complexes **1** and **2** was carried out using 1% agarose gel in TAE buffer (pH 8.2) and is presented in Fig. 9.

3.4.1. DNA cleavage in the absence of H_2O_2

Attempts were made to cleave DNA through the hydrolysis of the phosphodiester bond. Since this process does not require any external agents or light, it has biological significance. The DNA cleavage experiments were performed by exposing SC DNA to complexes **1** and **2** over a concentration range of 1–150 μM for 3 h in the absence of external agents (lanes 1–4, Fig. 9a and b for **1** and **2** respectively). The complexes show concentration dependent relaxation of SC DNA to the NC form. 90% conversion of SC DNA to NC form was achieved at 150 μM by **1** (Fig. 9a, lane 4), while in the case of **2**, 96% conversion was observed (Fig. 9b, lane 4).

To ensure that the copper complexes were solely responsible for the cleavage, control experiments were performed (Fig. 9c) under identical experimental conditions. Free $Cu(OAc)_2{\cdot}H_2O$, peptides and phen did not show any DNA cleavage activity, even after incubation for 3 h at a concentration of 1 mM. These results suggest that the complexes are responsible for the DNA cleavage and not the individual constituents, viz. free copper or the free ligands.

3.4.2. DNA cleavage in the presence of H_2O_2

The cleavage was monitored by treating SC DNA with **1** and **2** in the presence of H_2O_2 (lanes 5–6, Fig. 9a and b for **1** and **2** respectively). A control experiment using H_2O_2 alone did not show any significant DNA cleavage under similar experimental conditions (Fig. 9c, lane 8). This proves the catalytic role of **1** and **2** in the presence of H_2O_2. In the presence of H_2O_2, complex **1** converts ~89% of SC DNA into the NC form at a concentration of 10 μM, while complex **2** converts ~97% at a similar concentration.

The his-tyr system (**2**) shows higher cleavage activity than the his-trp system (**1**) due to the presence of a phenolic hydroxyl 'OH' functional group in the peptide side chain (his-tyr), which

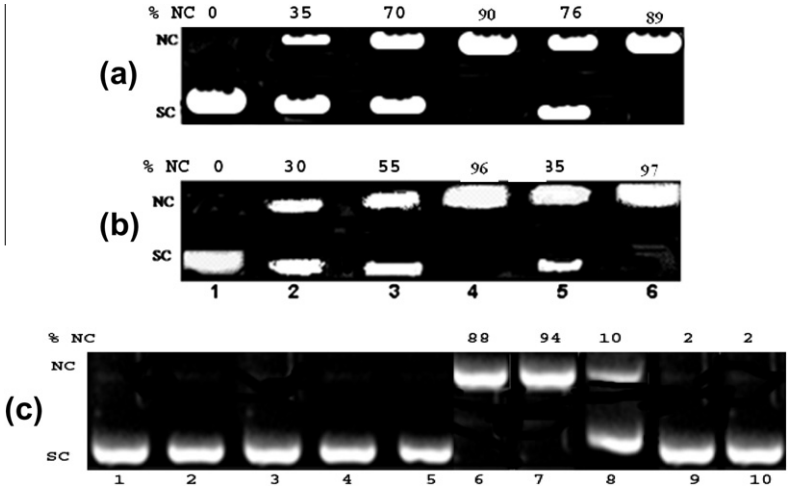

Fig. 9. Agarose gel electrophoresis pattern for the cleavage of supercoiled pUC19 DNA by **1** and **2** at 37 °C in a buffer containing 5 mM Tris. HCl/5 mM aq. NaCl. (a) Lane 1, DNA control; lane 2, DNA+ **1** (50 μM); lane 3, DNA+ **1** (100 μM); lane 4, DNA+ **1** (150 μM); lane 5, DNA+ **1** (5 μM) + H_2O_2 (1 mM); lane 6, DNA+ **1** (10 μM) + H_2O_2 (1 mM); (b) lane 1, DNA control; lane 2, DNA+ **2** (50 μM); lane 3, DNA+ **2** (100 μM); lane 4, DNA+ **2** (150 μM); lane 5, DNA+ **2** (5 μM) + H_2O_2 (1 mM); lane 6, DNA+ **2** (10 μM) + H_2O_2 (1 mM); (c) lane 1, DNA control; lane 2, DNA+ $Cu(OAc)_2{\cdot}H_2O$ (1 mM); lane 3, DNA+ his-trp (1 mM); lane 4, DNA+ his-tyr (1 mM); lane 5, DNA+ phen (1 mM); lane 6, DNA+ **1** (150 μM) + DMSO (1 mM); lane 7, DNA+ **2** (150 μM) + DMSO (1 mM); lane 8, DNA+ H_2O_2 (1 mM); lane 9, DNA+ **1** (10 μM) + H_2O_2 (1 mM) + DMSO (1 mM); lane 10, DNA+ **1** (10 μM) + H_2O_2 (1 mM) + DMSO (1 mM).

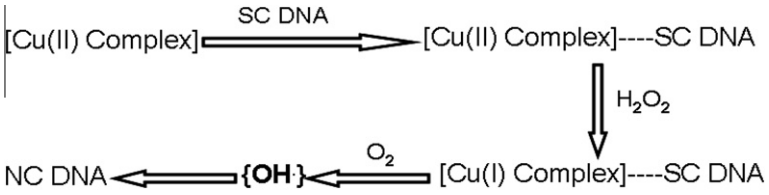

Scheme 2. A proposed mechanism for the oxidative cleavage of DNA by **1** and **2**.

Table 2
Percentage of hydrolytic and oxidative cleavage of DNA as a function of concentration of complexes.

Entry	Complex	Hydrolytic cleavage		Oxidative cleavage		Ref.
		[a][M]	[b]%Clea	[c][M]	[d]%Clea	
1	**1**	50, 100, 150	35, 70, 90	5, 10	76, 89	This work
2	**2**	50, 100, 150	30, 55, 96	5, 10	85, 97	This work
3	[Cu(trp-phe)(phen)(H_2O)]	5, 10, 25, 50, 100	15, 25, 45, 100, smear	–	–	[54]
4	[Cu(trp-phe)(phen)(H_2O)]	10, 25, 50, 100	5, 8, 15, 40	–	–	[54]
5	[Cu(his-leu)(phen)]	125, 187, 378, 437, 500	45, 54, 69, 95, 97	–	–	[16]
6	[Cu(his-ser)(phen)]	125, 187, 250, 312, 378, 437, 500	50, 53, 55, 60, 65, 85, 90	–	–	[16]
7	[Cu(Hist)(trp)]	125, 250, 375, 500, 625	21, 35, 42, 49, 53	–	–	[55]
8	[Cu(Hist)(tyr)]	125, 250, 375, 500, 625	12, 21, 32, 45, 56	–	–	[55]
9	[Cu(L-Val)(bipy)(H_2O)]	–	–	50	34	[56]
10	[Cu(L-Val)(phen)(H_2O)]	–	–	50	72	[56]
11	[Cu(L-Val)(dpq)(H_2O)]	–	–	50	86	[56]
12	[Cu(L-Val)(dppz)(H_2O)]	–	–	50	95	[56]

[a] Concentration of the copper(II) complexes in the absence of external agents.
[b] % of DNA cleavage (hydrolytic).
[c] Concentration of the copper(II) complexes in the presence of external agents (1 mM H_2O_2 for entries 1 and 2; 5 mM MPA for entries 9–12).
[d] % of DNA cleavage (oxidative).

shows a stronger hydrogen bonding interaction with the phosphate oxygen of the DNA backbone than the indole 'NH' hydrogen in the side chain (his-trp) of **1**, thereby enhancing the cleavage activity.

3.4.3. Mechanistic investigation of the DNA cleavage

In order to diagnose whether the cleavage mechanism followed a hydrolytic or oxidative pathway, we monitored the quenching of DNA cleavage in the presence of DMSO, a known hydroxyl radical scavenger. When SC DNA was incubated with the complexes at a concentration of 150 μM in the presence of DMSO, without adding external agents (such as H_2O_2), only slight inhibition (⟨2%⟩) of DNA cleavage was observed (Fig. 9c, lanes 6 and 7 for **1** and **2** respectively). This rules out the possibility of DNA cleavage via OH·-based depurination and also a possible oxidative cleavage pathway (dioxygen + copper complex + traces of DNA) [52]. Hence the complexes act as "self-activating agents" and cleave the ds-DNA by a hydrolytic mechanism.

On the other hand, in the presence of H_2O_2, the DNA cleavage was almost eliminated on addition of DMSO, indicating that hydroxyl radicals (OH·) are generated and initiated the cleavage process (Fig. 9c, lanes 9 and 10 for **1** and **2** respectively). On the basis of this observation, the mechanism of DNA cleavage mediated by **1** and **2** may be proposed as follows: DNA cleavage is redox-mediated – the complexes would first interact with DNA by intercalation to form a Cu(II)···DNA species, followed by its reduction by an external agent (H_2O_2) to a Cu(I)···DNA species, which then generates hydroxyl radicals on reaction with O_2. These hydroxyl radicals would then attack DNA, causing strand scission (Scheme 2). A similar pathway was proposed by Sigman for the oxidative cleavage reaction with the bis(phen)copper complex [53].

It may be seen from Table 2 [16,54–56] that the DNA binding and cleavage affinity of Cu(II)–amino acid complexes is less compared to Cu(II)–dipeptide complexes, in spite of the square pyramidal geometry which is known to enhance the cleavage activity around Cu(II) in the former complexes. Within the Cu–dipeptide complexes, those containing aromatic moieties bind and cleave DNA more effectively compared to their aliphatic

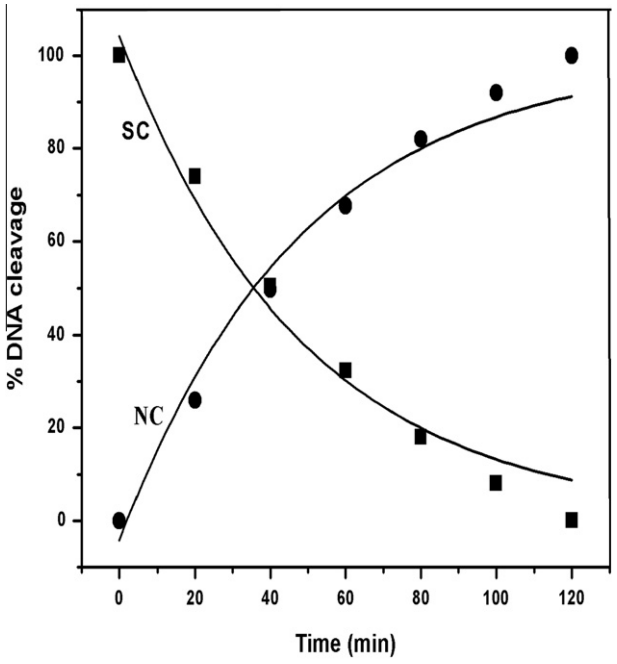

Fig. 10. Disappearance of the supercoiled form (SC) DNA and formation of the nicked circular (NC) form in the presence of complex **1**. Conditions: [complex] = 300 μM. Data points (■) refer to SC DNA and data points (●) refer to NC DNA.

analogs. For example, for the complete cleavage of DNA, about 500 μM concentration of $[Cu^{II}(HisLeu)(phen)]^+$ and $[Cu^{II}(HisSer)(phen)]^+$ were required, whereas a similar level of cleavage was achieved with only 150 μM concentration of the present complexes ([Cu(II)(boc(tos)-his-trp-ome)(phen)]$(ClO_4)_2$ (**1**) and [Cu(II)(boc(tos)-his-tyr-ome)(phen)]$(ClO_4)_2$ (**2**)). This clearly emphasizes the significance of aromatic moieties in DNA binding and cleavage.

3.4.4. Kinetics

After confirming the cleavage pathway, attention was focused towards the kinetic aspects of the cleavage. The kinetics of the cleavage reactions were studied by monitoring the % cleavage versus incubation time (Fig. 10 for **1**, Fig. S11 for **2**). The decrease and increase of SC and NC DNA forms were found to fit well to a single-exponential decay and increase, respectively. By curve fitting, the following hydrolysis rates for SC DNA were obtained at 37 °C at a fixed complex concentration of 300 μM: 1.70 h^{-1} ($R = 0.975$) for **1** and 1.82 h^{-1} ($R = 0.963$) for **2**. This amounts to a (4.7–5.0) $\times 10^7$-fold rate enhancement compared to non-catalyzed DNA cleavage (3.6×10^{-8} h^{-1}) [57], which is impressive considering the type of ligands and experimental conditions employed.

4. Conclusions

The synthesis, structural characterization, DNA binding and cleavage properties of ternary histidine based dipeptide Cu(II) complexes, [Cu(II)(boc(tos)-his-trp-ome)(phen)]$(ClO_4)_2$ (**1**) and [Cu(II)(boc(tos)-his-tyr-ome)(phen)]$(ClO_4)_2$ (**2**), are reported in this paper. The analytical and physicochemical data suggest that the complexes are arranged in a square-planar geometry around copper. The DNA binding results reveal that the complexes bind to DNA in an intercalation mode. Their cleavage activity on pUC19 plasmid DNA in the absence and presence of H_2O_2 show that they cleave DNA efficiently. Since the mixed-ligand complexes, containing bidentate histidine dipeptide and phen, show a unique ability to effect DNA double strand scission in both hydrolytic and oxidative cleavage reactions, they are considered as better DNA binding and cleavage agents, and hence artificial restriction enzymes in nucleic acid biochemistry.

Acknowledgments

P.R.R. thanks the Council of Scientific and Industrial Research (CSIR) and the University Grants Commission (UGC), New Delhi for financial support. N.R. thanks the CSIR for a Senior Research Fellowship.

Appendix A. Supplementary data

Supplementary data associated with this article can be found, in the online version, at http://dx.doi.org/10.1016/j.poly.2012.05.046.

References

[1] F. Mancin, P. Scrimin, P. Tecillab, U. Tonellato, Chem. Commun. (2005) 2540.
[2] R. Kramer, Coord. Chem. Rev. 182 (1999) 243.
[3] N.H. Williams, B. Takasaki, M. Wall, J. Chin, Acc. Chem. Res. 32 (1999) 485.
[4] E.L. Hegg, J.N. Burstyn, Coord. Chem. Rev. 173 (1998) 133.
[5] J.A. Cowan, Chem. Rev. 98 (1998) 1067.
[6] A. Sreedhara, J.A. Cowan, J. Biol. Inorg. Chem. 6 (2001) 337.
[7] A. Nori, J. Kopecek, Adv. Drug Delivery Rev. 57 (2005) 609.
[8] Y. Xie, G.G. Miller, S.A. Cubitt, K.J. Soderlind, M.J. Allalunis-Turner, J.W. Lown, Anticancer Drug Res. 12 (1997) 169.
[9] M. Shi, K. Ho, A. Keating, M.S. Shoichet, Adv. Funct. Mater. 19 (2009) 1689.
[10] H.T. Chifotides, K.R. Dunbar, Acc. Chem. Res. 38 (2005) 146.
[11] P.J. Bednarski, F.S. Mackay, P.J. Sadler, Anticancer Agents Med. Chem. 7 (2007) 75.
[12] P.J. Dyson, M.J. Rose, N.L. Fry, R. Marlow, L. Hinck, P.K. Mascharak, J. Am. Chem. Soc. 30 (2008) 8834.
[13] R. Gust, W. Beckb, G. Jaouenc, H. Schenberger, Coord. Chem. Rev. 253 (2009) 2742.
[14] N. Thanki, J.M. Thornton, J.M. Goodfellow, J. Mol. Biol. 202 (1998) 637.
[15] R.S. Kumar, S. Arunachalam, Eur. J. Med. Chem. 44 (2009) 1878.
[16] P.R. Reddy, P. Manjula, Chem. Biodiv. 4 (2007) 468.
[17] M. Bodanszky, A. Bodanszky, The Practices of Peptide Synthesis, Springer, New York, 1984.
[18] B.N. Figgi's, J. Lewis, in: J. Lewis, R.C. Wilkinson (Eds.), Modern Coordination Chemistry, Wiley Interscience, New York, 1967.
[19] J. Marmur, J. Mol. Biol. 3 (1961) 208.
[20] M.E. Reichmann, C.A. Rice, C.A. Thomos, P. Doty, J. Am. Chem. Soc. 76 (1954) 3047.
[21] F. Garland, D.E. Graves, L.W. Yielding, H.C. Cheung, Biochemistry 19 (1980) 3221.
[22] J. He, P. Hu, Y.-J. Wang, M.-L. Tong, H. Sun, Z.-W. Mao, L.-N. Ji, Dalton Trans. (2008) 3207.
[23] C.V. Kumar, E.H. Asuncion, J. Am. Chem. Soc. 115 (1993) 8547.
[24] A. Wolfe, G.H. Shimer, T. Meehan, Biochemistry 26 (1987) 6392.
[25] J.B. Lepecq, C. Paoletti, J. Mol. Biol. 27 (1967) 87.
[26] R.N. Patel, N. Singh, V.L.N. Gundla, Indian J. Chem., Sect. A 45 (2006) 614.
[27] K. Nakamoto, Infrared and Raman Spectra of Inorganic and Coordination Compounds, third ed., John Wiley & Sons, New York, 1978, p. 228.
[28] P.P. Silva, W. Guerra, J.N. Silveira, A.M.C. Ferreira, T. Bortolotto, F.L. Fischer, H. Terenzi, A. Neves, E.C. Pereira-Maia, Inorg. Chem. 50 (2011) 6414.
[29] G.G. Mohamed, M.M. Omar, A.M.M. Hindy, Spectrochim. Acta, Part A 62 (2005) 1140.
[30] A.B.P. Lever, Inorganic Electronic Spectroscopy, Elsevier, New York, 1984.
[31] S.-D. Choi, M.-S. Kim, S.K. Kim, P. Lincoln, E. Tuite, B. Norden, Biochemistry 36 (1997) 214.
[32] I. Ortmans, B. Elias, J.M. Kelly, C. Moucheron, A.K. Demesmaeker, Dalton Trans. (2004) 668.
[33] M. Cory, D.D. Mckee, J. Kagan, D.W. Henry, J.A. Miller, J. Am. Chem. Soc. 107 (1985) 2528.
[34] A. Ambroise, B.G. Maiya, Inorg. Chem. 39 (2000) 4256.
[35] P.U. Maheswari, M. Palaniandavar, J. Inorg. Biochem. 98 (2004) 219.
[36] F. Gao, H. Chao, F. Zhou, Y.X. Yuan, B. Peng, L.N. Ji, J. Inorg. Biochem. 100 (2006) 1487.
[37] R.B. Nair, E.S. Teng, S.L. Kirkland, C.J. Murphy, Inorg. Chem. 37 (1998) 139.
[38] S.A. Tysoe, R.J. Morgan, A.D. Baker, T.C. Strekas, J. Phys. Chem. 97 (1993) 1707.
[39] T.M. Kelly, A.B. Tossi, D.J. McConnell, T.C. Strekas, Nucleic Acids Res. 13 (1985) 6017.
[40] H.M. Berman, P.R. Young, Annu. Rev. Biophys. Bioeng. 10 (1981) 87.
[41] T.A. Tysoc, A.D. Baker, T.C. Strekas, J. Phys. Chem. 97 (1993) 1707.
[42] W.D. Wilson, L. Ratmeyer, M. Zhao, L. Strekowski, D. Boykin, Biochemistry 32 (1993) 4098.
[43] Y. Li, Y. Wu, J. Zhao, P. Yang, J. Inorg. Biochem. 101 (2007) 283.
[44] S. Satyanarayana, J.C. Dabrowiak, J.B. Chaires, Biochemistry 32 (1993) 2573.
[45] L.N. Ji, X.H. Zou, J.G. Liu, Coord. Chem. Rev. 216–217 (2001) 513.
[46] S. Satyanarayana, J.C. Dabrowiak, J.B. Chaires, Biochemistry 31 (1992) 9319.
[47] C.V. Kumar, J.K. Barton, N.J. Turro, J. Am. Chem. Soc. 107 (1985) 5518.
[48] J.R. Lakowicz, G. Webber, Biochemistry 12 (1973) 4161.
[49] H. Arkawa, R. Ahmad, M. Naoui, H.A. Tajmir-Riahi, J. Biol. Chem. 275 (2000) 10150.
[50] M. Howe-Grant, K.C. Wu, W.R. Bauer, S.J. Lippard, Biochemistry 15 (1976) 4339.
[51] E. Gao, L. Liu, M. Zhu, Y. Huang, F. Guan, X. Gao, M. Zhang, L. Wang, W. Zhang, Y. Sun, Inorg. Chem. 50 (2011) 4732.
[52] R. Ren, P. Yang, W. Zheng, Z. Hua, Inorg. Chem. 39 (2000) 5454.
[53] D.S. Sigman, Acc. Chem. Res. 19 (1986) 180.
[54] P.R. Reddy, N. Raju, B. Satyanarayana, Chem. Biodiv. 8 (2011) 131.
[55] P.R. Reddy, K.S. Rao, B. Satyanarayana, Tetrahedron Lett. 47 (2006) 7311.
[56] A.K. Patra, A.R. Chakravarthy, Proc. Indian Natl. Sci. Acad. 73 (2007) 157.
[57] A. Roigk, R. Hettich, H.-J. Schneider, Inorg. Chem. 37 (1998) 751.